

AN INTRIGUING CHROMOSPHERIC JET OBSERVED BY *Hinode*: FINE STRUCTURE KINEMATICS AND EVIDENCE OF UNWINDING TWISTS

WEI LIU^{1,2}, THOMAS E. BERGER¹, ALAN M. TITLE¹, AND THEODORE D. TARBELL¹

¹ Lockheed Martin Solar and Astrophysics Laboratory, Department ADBS, Building 252, 3251 Hanover Street, Palo Alto, CA 94304, USA

² W. W. Hansen Experimental Physics Laboratory, Stanford University, Stanford, CA 94305, USA

Received 2009 September 5; accepted 2009 October 27; published 2009 November 19

ABSTRACT

We report a chromospheric jet lasting for more than 1 hr observed by the *Hinode* Solar Optical Telescope in unprecedented detail. The ejection occurred in three episodes separated by 12–14 minutes, with the amount and velocity of material decreasing with time. The upward velocities range from 438 to 33 km s⁻¹, while the downward velocities of the material falling back have smaller values (mean: -56 km s⁻¹) and a narrower distribution (standard deviation: 14 km s⁻¹). The average acceleration inferred from parabolic spacetime tracks is 141 m s⁻², a fraction of the solar gravitational acceleration. The jet consists of fine threads (0'.5–2'' wide), which exhibit coherent, oscillatory transverse motions perpendicular to the jet axis and about a common equilibrium position. These motions propagate upward along the jet, with the maximum phase speed of 744 ± 11 km s⁻¹ at the leading front of the jet. The transverse oscillation velocities range from 151 to 26 km s⁻¹, amplitudes from 6.0 to 1.9 Mm, and periods from 250 to 536 s. The oscillations slow down with time and cease when the material starts to fall back. The falling material travels along almost straight lines in the original direction of ascent, showing no transverse motions. These observations are consistent with the scenario that the jet involves untwisting helical threads, which rotate about the axis of a single large cylinder and shed magnetic helicity into the upper atmosphere.

Key words: Sun: atmospheric motions – Sun: chromosphere – Sun: corona – Sun: flares – Sun: transition region

Online-only material: animations

1. INTRODUCTION

Transient, small-scale ejections of plasma from the lower atmosphere are common manifestations of solar activity. Cool plasma ejections were observed as emission in H α or absorption at other wavelengths and historically called surges (Newton 1934). Hot ejections were usually called jets and observed as emission in ultraviolet (Brueckner & Bartoe 1983), extreme ultraviolet (EUV; Alexander & Fletcher 1999), and soft X-rays (Shibata et al. 1992; Strong et al. 1992). Some observations (Schmieder et al. 1988; Chae et al. 1999; Jiang et al. 2007) have indicated that cool surges and hot jets are closely related in space and time, but their physical relationship has not been established. Torsional motions or helical features have long been seen in surges or jets (e.g., Xu et al. 1984; Kurokawa et al. 1987; Shimojo et al. 1996; Patsourakos et al. 2008), while their exact causes remain unclear. From now on, we refer to both surges and jets with a general term “jets”, unless otherwise noted.

Solar jets are commonly associated with flux emergence (Roy 1973b) or moving magnetic features (Gaizauskas 1982; Brooks et al. 2007). Models involving magnetic reconnection have thus been proposed (e.g., Rust 1968; Yokoyama & Shibata 1995). Mechanisms (see review in Canfield et al. 1996) suggested for accelerating jet material to 10–1000 km s⁻¹ include reconnection outflows driven by the slingshot effect of magnetic tension (Yokoyama & Shibata 1995), the pressure gradient behind the shock formed by reconnection outflows (Yokoyama & Shibata 1996; Tarbell et al. 1999), chromospheric evaporation caused by heating from the associated flare (Shimojo & Shibata 2000), and relaxation of magnetic twists (Shibata & Uchida 1985).

Hinode (Kosugi et al. 2007), with its superior resolutions, has provided unprecedented details and spurred renewed interest in solar jets. They were found to be ubiquitous on various spatial and temporal scales in the Ca II H line (Shibata et al. 2007;

Nishizuka et al. 2008), EUV (Culhane et al. 2007; Moreno-Insertis et al. 2008), and soft X-rays (Savcheva et al. 2007; Nitta et al. 2008). In this Letter, we report an intriguing jet observed by *Hinode* in great detail, and attempt to obtain new clues to some unanswered questions mentioned above.

2. OBSERVATIONS AND DATA ANALYSIS

The chromospheric jet under study occurred from 02:40 to 04:20 UT on 2007 February 9 on the west limb, accompanied by a *GOES* A4.9 flare. It was observed by the Solar Optical Telescope (SOT; Tsuneta et al. 2008) and X-Ray Telescope on board *Hinode*, and by *TRACE*, *STEREO*, *RHESSI*, and several ground-based observatories. The SOT observations were obtained in the Ca II H line passband, sensitive to chromospheric temperatures of 1–2 × 10⁴ K. The high spatial resolution (~0'.2) and cadence (8 s) allowed us to investigate the fine structures and kinematics of the jet, which are the focus of this Letter. A comprehensive study of this event using multiwavelength data will be presented in the future. We processed Ca images with the standard `fg_prep` routine, and cross-correlated neighboring images to correct for pointing drifts, with a subarcsecond accuracy over a 2 hr duration. The absolute solar coordinates were determined by fitting the limb and are thus approximate with uncertainties in the roll angle. We then applied a radial filter to reduce the contrast between the bright disk and faint emission above the limb, and finally deconvolved the images with the SOT point-spread function determined using the lunar limb during eclipses (C. DeForest 2009, private communication) to sharpen fine features.

A sample of the resulting images is rotated clockwise by 90° and plotted in Figure 1, showing the evolution of the jet. We find that the precursor of the jet appeared at 02:40 UT as a bundle of fine material threads (typical widths: 0'.5–2'')

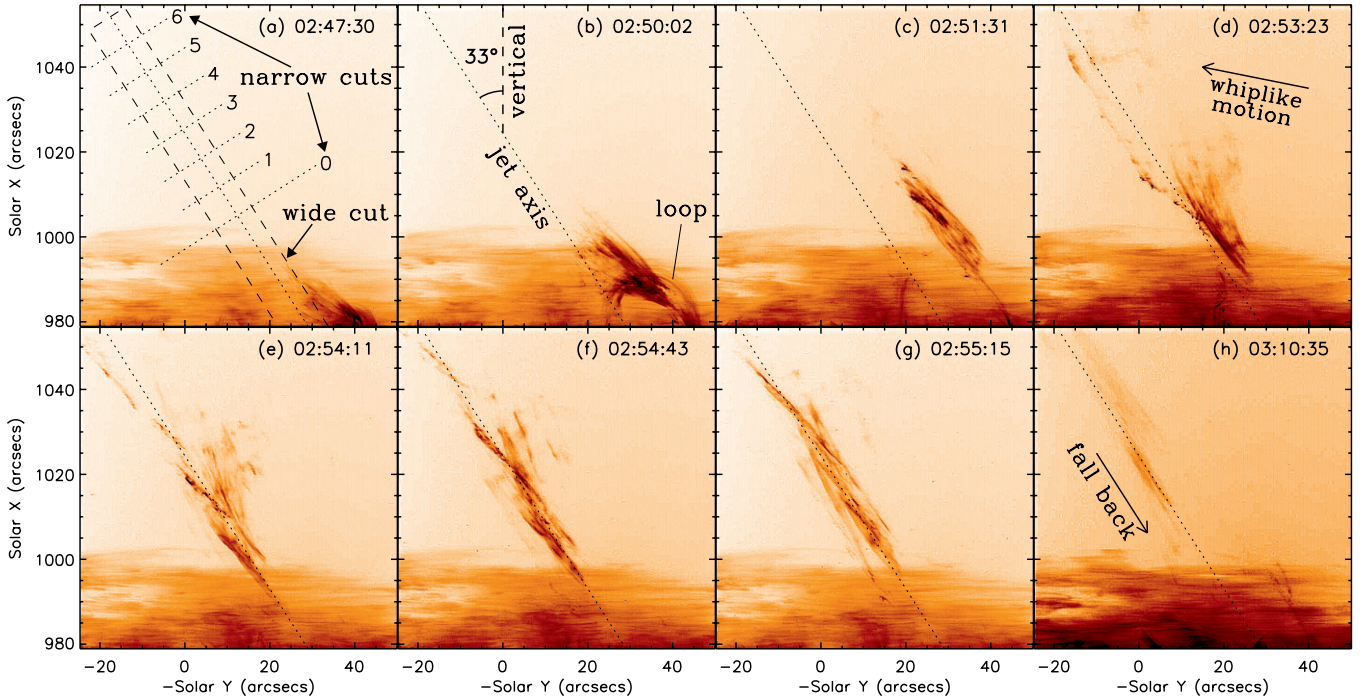


Figure 1. Negative *Hinode* Ca II H images. The diagonal dotted line marks the jet axis. The dashed box indicates a $10''$ wide cut along the axis for the time–distance diagram shown in Figure 2(a), while the numbered dotted lines represent $1''$ narrow cuts perpendicular to the axis (see movie 1 in the online version of the journal). (An animation of this figure is available in the online journal.)

at $\sim 40^\circ$ from the photosphere extending to a height of $\sim 20''$. With these threads exhibiting oscillatory transverse motions across its axis, this bundle rose up, first gradually and then rapidly, and a loop grew simultaneously (Figure 1(b)). At 02:51:31 UT, the bundle started to swing back to the left in a whip-like manner (Figure 1(d)), similar to that in simulated cool (10^4 K) jets (Yokoyama & Shibata 1995). Meanwhile, with their transverse motions continuing, the threads were ejected upward (Figures 1(d)–(g)). Later in the event up to 04:20 UT, material bound by gravity fell back to the chromosphere along the original paths of ascent. In contrast to those of the ascending material, the streamlines of the falling material were almost straight lines, with no detectable transverse motions (Figure 1(h)). To quantify the kinematics of the jet, we constructed an orthogonal coordinate system based on the jet orientation. We first visually determined the axis passing through the center of the jet when it was fully developed and collimated (e.g., Figure 1(g)). This axis (dotted diagonal line in Figure 1) is located in the sky plane and at 33° from the local vertical on the equator, and its intersection with the photosphere is defined as the origin O for measuring the distance s_{\parallel} along the jet. We used a $10''$ wide cut (dashed box in Figure 1(a)) along the axis, and averaged pixels across the width to obtain the time–distance diagram for the axial motions. Likewise, we selected seven narrow cuts ($1''$ wide, numbered 0–6) perpendicular to and centered at the jet axis to study the transverse motions. These narrow cuts are uniformly spaced by $8''$ and Cut 0 is positioned at $s_{\parallel} = 39''$ from O . The distance s_{\perp} across the jet along the narrow cuts is measured from upper right to lower left in Figure 1(a) with $s_{\perp} = 0$ located at the jet axis.

2.1. Axial Motions Along Jet

The axial motions of material along the jet are represented by the time–distance diagram (Figure 2(a)) from the wide cut. The

upward (downward) tracks correspond to ascending (falling) material. Some tracks show deceleration and change from upward to downward within the SOT field of view (FOV). We visually identified all unambiguous, straight-shaped portions of upward tracks just before deceleration and of downward tracks at the lowest altitudes where they are visible. We fitted these tracks linearly and show the fits and velocities in Figures 2(a) and (b).

As is evident, there are three episodes of material ejections, separated by 12–14 minutes. The number of tracks and amount of material of these episodes decrease with time; so do the mean and scatter of the upward velocities. During the first episode alone, the velocity rapidly decreases from 438.3 ± 0.4 to 33 ± 1 km s $^{-1}$ within 9 minutes. The mean and standard deviation of all the upward velocities are 119 and 109 km s $^{-1}$, respectively. In contrast, for the falling material, the downward velocities have less distinct episodes with a much smaller mean and scatter, and these values are -56 and 14 km s $^{-1}$ (Figures 2(b) and (e)).

For those tracks showing clear concave curvatures (see Figure 2(c)), we fitted their positions with a parabolic function of time t ,

$$s_{\parallel}(t) = s_{\parallel 0} + v_{\parallel 0}t - \frac{g_{\text{eff}}}{2}t^2, \quad (1)$$

where g_{eff} is the effective gravitational acceleration, and $s_{\parallel 0}$ and $v_{\parallel 0}$ are the initial position and velocity at $t = 0$. The fitted values of g_{eff} (Figures 2(d) and (f)) have a mean and standard deviation of 141 and 35 m s $^{-2}$, respectively. The component of the solar gravitational acceleration along the jet axis ranges from 231 m s $^{-2}$ at the photosphere to 197 m s $^{-2}$ at the top of the FOV (radial position $r = 1054''$). Our fitted g_{eff} is only a fraction of these values. Possible explanations for this apparent discrepancy include that (1) the jet is likely to be oriented out of the sky plane due to the line-of-sight effect, such that the discrepancy would be smaller, and (2) the force driving the

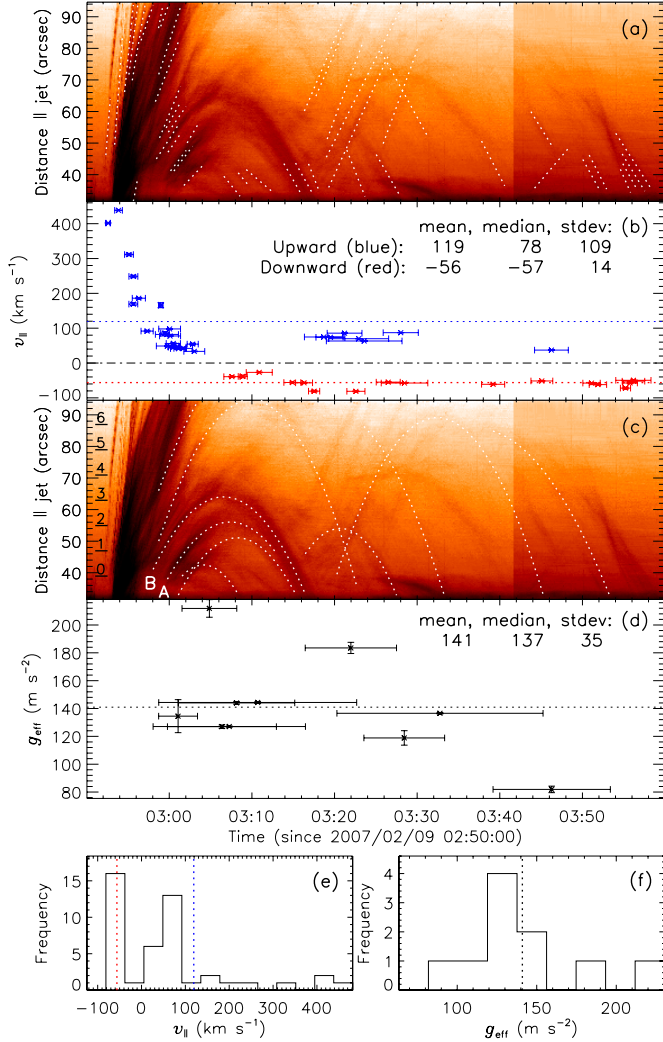


Figure 2. Kinematics along the jet. (a) Time–distance diagram of Ca intensity from the wide cut shown in Figure 1(a), overlaid with linear fits to individual tracks (see movie 2 in the online version of the journal). The increase in the background level at 03:41:40 UT is due to the pointing jump toward the disk center that possibly resulted in more scattered light in the telescope. (b) Velocities of the above fits vs. time. The horizontal bars indicate the time intervals of the fits. The horizontal dotted lines mark the means of the upward (>0) and downward (<0) velocities. (c) Same as (a) but overlaid with parabolic fits to selected tracks. The short bar underneath each number (0–6) on the left marks the position of the corresponding narrow cut shown in Figure 1(a). (d) Same as (b) but for the effective gravitational acceleration g_{eff} inferred from the fits in (c). (e and f) Histograms of the quantities shown in (b) and (d), with the means marked by the same dotted lines.

(An animation of this figure is available in the online journal.)

mass ejection, possibly at lower levels late in the event, could still reduce the effect of gravity. Note that Roy (1973a) also found in H α surges the acceleration of falling material being less than free fall, but the deceleration of ascending material being greater than gravity alone.

2.2. Transverse Motions Across Jet

The time–distance plot (Figure 3) from the narrow cuts clearly shows oscillatory transverse motions perpendicular to the jet during the first episode of material ejection. These oscillations propagate along the jet to higher altitudes, as indicated by the time delays across different cuts. We identified the first inverted-V-shaped track in each panel, and by linearly fitting the axial positions s_{\parallel} of the cuts versus the occurrence times

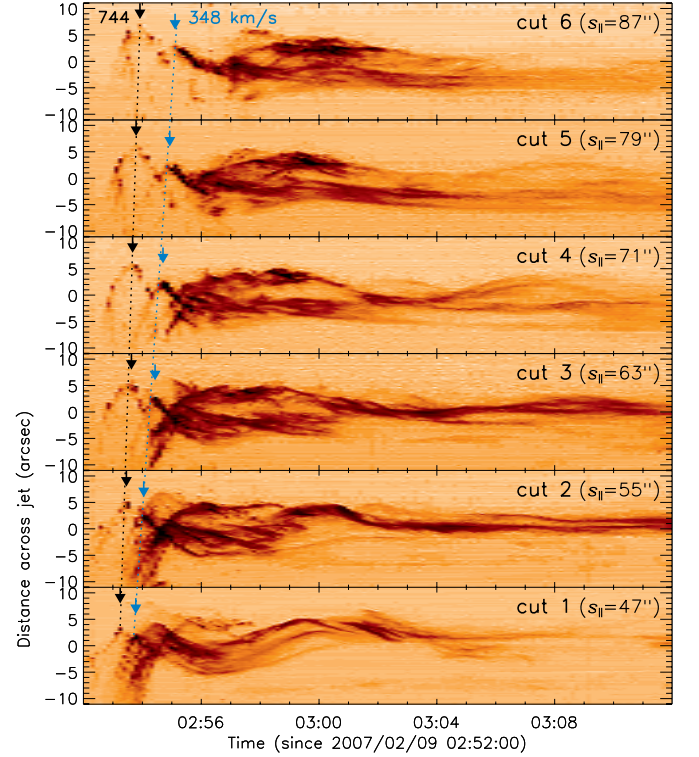


Figure 3. Time–distance diagram from 1'' narrow Cuts 1–6 perpendicular to the jet shown in Figure 1(a). The two arrows in each panel point to the crests of the first two inverted-V-shaped tracks, indicating delays toward higher altitudes. The dotted lines are linear fits to the delays; the resulting phase speeds are labeled.

of the track crest (indicated by the dark arrows), we obtained a phase speed of $v_{\text{ph}} = 744 \pm 11 \text{ km s}^{-1}$. The propagation of the second such track (indicated by the blue arrows) is 50% slower at $v_{\text{ph}} = 348 \pm 5 \text{ km s}^{-1}$. We also note that the oscillation amplitude decreases with time in each cut. At a higher cut, the separations between the threads become larger and various phase delays appear in their oscillations.

To quantify the transverse oscillations, we used the time–distance plot of Cut 0 as an example (Figure 4(a)), in which such motions are the most pronounced. We fitted the piecewise oscillatory tracks with a damped sine function:

$$s_{\perp}(t) = s_{\perp 0} + A(t) \sin \left[2\pi \int_{t_0}^t \frac{d\xi}{P(\xi)} \right] \\ = s_{\perp 0} + A(t) \sin \left[2\pi \tau_P \left(\frac{1}{P_0} - \frac{1}{P(t)} \right) \right], \quad (2)$$

where $A(t) = A_0 \exp[-(t - t_0)/\tau_A]$ is the amplitude and $P(t) = P_0 \exp[(t - t_0)/\tau_P]$ is the period, with τ_A and τ_P being their damping time. We find a rapid oscillation at the beginning of the event, corresponding to the rise and whip-like swing of the entire bundle mentioned earlier. The fitted transverse velocity at the equilibrium position near the middle of this track duration is $v_{\perp} = 151 \pm 6 \text{ km s}^{-1}$, and the amplitude and period at $t = t_0$ are $A_0 = 6.0 \pm 0.2 \text{ Mm}$ and $P_0 = 250 \pm 6 \text{ s}$. This is followed by a slower oscillation with the amplitude halved and the period doubled, giving a velocity of $v_{\perp} = 34 \pm 2 \text{ km s}^{-1}$. We also moved the 1'' narrow cut with time along the jet axis to keep up with the upward moving material and to remove the effect of its axial motion. The time–distance diagrams of such co-moving Cuts A and B are shown in Figures 4(b) and (c) for

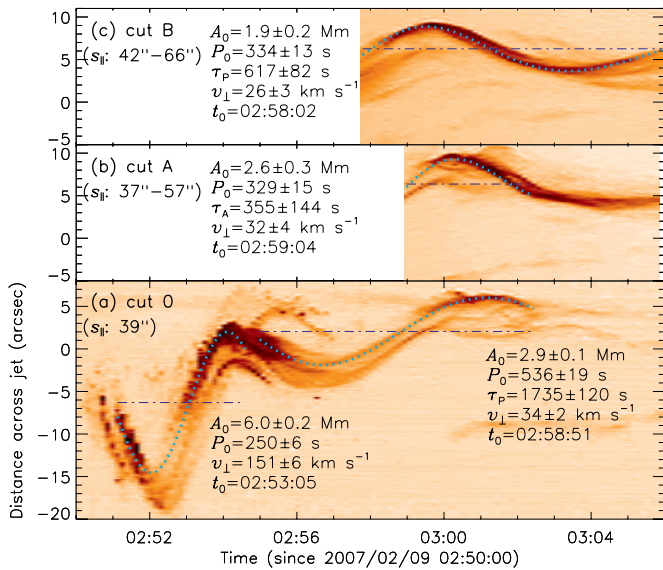


Figure 4. Same as Figure 3 but (a) for Cut 0 shown in Figure 1(a); (b) and (c) for cuts co-moving with the ascending material on the upward tracks A and B shown in Figure 2(c). The ranges of the cut position $s_{||}$ along the jet axis are labeled. The dotted lines are fits to fine tracks with a damped sine function (see the text), whose parameters are shown in the legends (with τ_A or $\tau_P = \infty$ omitted). The dot-dashed lines mark the fitted equilibrium positions.

the upward tracks A and B marked in Figure 2(c), respectively. Their damped sine fits yield transverse velocities similar to that of the second oscillation of the stationary Cut 0 noted here.

3. DISCUSSIONS

The simplest and most intuitive scenario that can tie together the above observations is that the jet is composed of helical threads undergoing untwisting spins, as proposed by Shibata & Uchida (1985, 1986) and Canfield et al. (1996). In this scenario, a highly twisted emerging flux rope or existing filament reconnects with less twisted “open” field lines, along which the stored twists and magnetic helicity are transported to the upper atmosphere. We interpret our observations in this framework as follows.

Chirality. The alternate and mutual shadowing of multiple threads consistently over time suggests that the threads oriented as crossing the jet axis from lower right to upper left are on the front side (closer to the observer), while those crossing from lower left to upper right are on the far side (Figures 1(d)–(g)). These threads, assumed to represent magnetic field lines, are thus left-handed screws. The former threads are seen to traverse the jet axis from left to right, while the latter from right to left. Their transverse motions (see movie 1 in the online version of the journal) are thus counterclockwise rotations when looking from above along the jet axis. The trajectories of the material, considering its upward axial motion, are thus right-handed helices. This is consistent with the unwinding of twisted field lines of the opposite handedness inferred here, as indicated by surge observations (Canfield et al. 1996; Jibben & Canfield 2004) and three-dimensional MHD simulations (Pariat et al. 2009).

Oscillatory transverse motions³ across the jet, in general, can be understood as the projections of rotations about an

axis in the sky plane. The initial rotation of the entire bundle, in particular, appears in a counterclockwise coning manner, and its velocity $v_{\perp} = 151 \pm 6 \text{ km s}^{-1}$ is fivefold greater than the other rotations during this event, but comparable to the 120 km s^{-1} velocity of whip-like or transverse motions reported for surges or jets (Canfield et al. 1996; Shimojo et al. 2007). The rest of the rotational velocities around 30 km s^{-1} and periods in the 330–540 s range are comparable to those of transverse oscillations found in X-ray jets (Cirtain et al. 2007), prominences (Okamoto et al. 2007), and coronal loops (Ofman & Wang 2008), which were interpreted as signatures of transverse MHD or Alfvén waves. The angular velocities inferred from Doppler measurements in H α surges are on the order of $10^{-3} \text{ rad s}^{-1}$ (Xu et al. 1984; Gu et al. 1994; Jibben & Canfield 2004), which translates to a period of $6 \times 10^3 \text{ s}$. These rotations are 10 times slower than reported here, although their axial velocities are only fractionally smaller.

Axial motions. Propagating torsional Alfvén waves associated with unwinding twists can explain the observed delays of the transverse motions with distance along the jet. The initial phase speed $v_{\text{ph}} = 744 \pm 11 \text{ km s}^{-1}$ (Figure 3) would correspond to the untwisting front or progressing pinch front which, according to Shibata & Uchida (1985), propagates at the Alfvén speed. Proposed driving mechanisms of jet material also include torsional Alfvén waves (Pariat et al. 2009) and the $\mathbf{J} \times \mathbf{B}$ force in the untwisting helices (Shibata & Uchida 1985). The decrease with time of the upward velocities as shown in Figures 2(a)–(b) indicates that the pitch spacing between adjacent helical threads increases with height. This is consistent with the expected axial expansion of unwinding screws.

Temporal evolution. We find a slowdown of the transverse motions (see Figures 3 and 4), which accompanies the decrease of the axial velocity (Figure 2(b)). In particular, when the rotations of Cuts A and B stop (Figures 4(b) and (c)) near 03:06–03:08 UT, the corresponding ascending material reaches its maximum height and starts to fall back. On its return, the material follows paths that are almost straight lines (until $\sim 20''$ above the photosphere) along the jet axis and shows no detectable transverse motions. Assuming the paths are along magnetic field lines, this means very little or no twist in the post-eruption field. This provides further evidence for the causal link between the jet and unwinding twists and for the role played by the jet in shedding away twists or magnetic helicity.

An alternative to our rotation interpretation is planar waves, which seem, however, difficult as an explanation of some of the observations (see movie 1 in the online version of the journal): (1) multiple threads are seen to undergo coherent, oscillatory transverse motions, one following another with consistent phase delays and reversing their direction of motion at roughly the same distance from the jet axis. This is consistent with surge observations (Canfield et al. 1996) and can be readily understood if these threads are distributed on a single rotating cylindrical surface. (2) Likewise, some sheet-shaped material volumes periodically change their appearances in a way as if they are on the surface of a rotating cylinder. To distinguish between these two interpretations with certainty, simultaneous high-resolution Ca images and H α Doppler measurements are needed and can both be obtained with SOT (but unavailable for this event).

4. CONCLUSIONS

We have presented kinematic measurements of both axial and transverse motions of a chromospheric jet observed by *Hinode* SOT at high spatial and temporal resolutions. This study

³ The apparent transverse motions at Cuts 1–6 shown in Figure 3 result from the rotation about and the translation along the jet axis of individual unwinding helical threads. However, at the lowest narrow cut (Cut 0), since the bundle of threads is packed as a whole and extends almost parallel to the jet axis, Figure 4(a) represents mainly the true rotation of the entire bundle. So do Figures 4(b) and (c) for the co-moving cuts.

complements previous low-resolution counterparts of H α surges and EUV or X-ray jets, and offers new insights to this type of phenomena. Our major results and interpretations are as follows.

1. The ejection occurs in three episodes separated by 12–14 minutes, rather than continuously. The amount and velocity of ejected material decrease with time. The ejecting velocities have a wide range from 438 to 33 km s⁻¹, while the velocities of material falling back have a narrow range (mean: -56 km s⁻¹ and standard deviation: 14 km s⁻¹). The acceleration inferred from parabolic tracks in the time–distance diagram has a mean of 141 m s⁻², a fraction of the solar gravitational acceleration.
2. The jet consists of 0'.5–2'' thick fine threads, which exhibit oscillatory transverse motions across the jet about a common equilibrium position. These oscillations have velocities ranging from 151 ± 6 to 26 ± 3 km s⁻¹, amplitudes from 6.0 ± 0.2 to 1.9 ± 0.2 Mm, and periods from 250 ± 6 to 536 ± 19 s. The upward propagation of the oscillations has a maximum phase speed of 744 ± 11 km s⁻¹ (comparable to the coronal Alfvén speed) associated with the leading front of the jet.
3. The oscillatory transverse motions slow down with time and cease near the time when the material reaches its maximum height and starts to fall back. The falling material travels along almost straight lines in the original direction of ascent, showing no more signatures of transverse motions.
4. These observations are consistent with the scenario that the jet involves unwinding of left-handed helical threads that rotate counterclockwise about a common axis. The untwisting wave front propagates upward at the Alfvén speed. The pitch spacing between adjacent helical threads increases with height, consistent with the expected axial expansion of unwinding screws. The jet results in magnetic helicity being shed into the upper atmosphere.

A more in-depth multiwavelength study of this event and comparison with theoretical models are underway and will be published in the future.

Many thanks to Richard Shine, Tong-Jiang Wang, T. J. Okamoto, and Alexey Kruglov. This work was supported by *Hinode* SOT contract NNM07AA01C. *Hinode* is a Japanese mission developed and launched by ISAS/JAXA, with NAOJ as domestic partner and NASA and STFC (UK) as international partners. It is operated by these agencies in cooperation with ESA and NSC (Norway).

REFERENCES

- Alexander, D., & Fletcher, L. 1999, *Sol. Phys.*, **190**, 167
- Brooks, D. H., Kurokawa, H., & Berger, T. E. 2007, *ApJ*, **656**, 1197
- Brueckner, G. E., & Bartoe, J.-D. F. 1983, *ApJ*, **272**, 329
- Canfield, R. C., Reardon, K. P., Leka, K. D., Shibata, K., Yokoyama, T., & Shimojo, M. 1996, *ApJ*, **464**, 1016
- Chae, J., Qiu, J., Wang, H., & Goode, P. R. 1999, *ApJ*, **513**, L75
- Cirtain, J. W., et al. 2007, *Science*, **318**, 1580
- Culhane, L., et al. 2007, *PASJ*, **59**, 751
- Gaizauskas, V. 1982, *Adv. Space Res.*, **2**, 11
- Gu, X. M., Lin, J., Li, K. J., Xuan, J. Y., Luan, T., & Li, Z. K. 1994, *A&A*, **282**, 240
- Jiang, Y. C., Chen, H. D., Li, K. J., Shen, Y. D., & Yang, L. H. 2007, *A&A*, **469**, 331
- Jibben, P., & Canfield, R. C. 2004, *ApJ*, **610**, 1129
- Kosugi, T., et al. 2007, *Sol. Phys.*, **243**, 3
- Kurokawa, H., Hanaoka, Y., Shibata, K., & Uchida, Y. 1987, *Sol. Phys.*, **108**, 251
- Moreno Inertis, F., Galsgaard, K., & Ugarte-Urra, I. 2008, *ApJ*, **673**, L211
- Newton, H. W. 1934, *MNRAS*, **94**, 472
- Nishizuka, N., Shimizu, M., Nakamura, T., Otsuji, K., Okamoto, T. J., Katsukawa, Y., & Shibata, K. 2008, *ApJ*, **683**, L83
- Nitta, N. V., Mason, G. M., Wiedenbeck, M. E., Cohen, C. M. S., Krucker, S., Hannah, I. G., Shimojo, M., & Shibata, K. 2008, *ApJ*, **675**, L125
- Ofman, L., & Wang, T. J. 2008, *A&A*, **482**, L9
- Okamoto, T. J., et al. 2007, *Science*, **318**, 1577
- Pariat, E., Antiochos, S. K., & DeVore, C. R. 2009, *ApJ*, **691**, 61
- Patsourakos, S., Pariat, E., Vourlidas, A., Antiochos, S. K., & Wuelser, J. P. 2008, *ApJ*, **680**, L73
- Roy, J. R. 1973a, *Sol. Phys.*, **32**, 139
- Roy, J. R. 1973b, *Sol. Phys.*, **28**, 95
- Rust, D. M. 1968, in IAU Symp. 35, Structure and Development of Solar Active Regions, ed. K. O. Kiepenheuer (Dordrecht: Kluwer), 77
- Savcheva, A., et al. 2007, *PASJ*, **59**, 771
- Schmieder, B., Mein, P., Simnett, G. M., & Tandberg-Hanssen, E. 1988, *A&A*, **201**, 327
- Shibata, K., & Uchida, Y. 1985, *PASJ*, **37**, 31
- Shibata, K., & Uchida, Y. 1986, *Sol. Phys.*, **103**, 299
- Shibata, K., et al. 1992, *PASJ*, **44**, L173
- Shibata, K., et al. 2007, *Science*, **318**, 1591
- Shimojo, M., Hashimoto, S., Shibata, K., Hirayama, T., Hudson, H. S., & Acton, L. W. 1996, *PASJ*, **48**, 123
- Shimojo, M., & Shibata, K. 2000, *ApJ*, **542**, 1100
- Shimojo, M., et al. 2007, *PASJ*, **59**, 745
- Strong, K. T., Harvey, K., Hirayama, T., Nitta, N., Shimizu, T., & Tsuneta, S. 1992, *PASJ*, **44**, 461
- Tarbell, T., Ryutova, M., Covington, J., & Fludra, A. 1999, *ApJ*, **514**, L47
- Tsuneta, S., et al. 2008, *Sol. Phys.*, **249**, 167
- Xu, A.-A., Ding, J.-P., & Yin, S.-Y. 1984, *Acta Astron. Sin.*, **25**, 119
- Yokoyama, T., & Shibata, K. 1995, *Nature*, **375**, 42
- Yokoyama, T., & Shibata, K. 1996, *PASJ*, **48**, 353